ACS SENSORS

pubs.acs.org/acssensors

Article

Point-of-Care Blood Coagulation Assay Based on Dynamic Monitoring of Blood Viscosity Using Droplet Microfluidics

Linzhe Chen, Donghao Li, Xinyu Liu, Yihan Xie, Jieying Shan, Haofan Huang, Xiaxia Yu, Yudan Chen, Weidong Zheng, and Zida Li*

Cite This: https://doi.org/10.1021/acssensors.1c02360

Read Online

ACCESS | Metrics & More | Article Recommendations | Supporting Information

ABSTRACT: Monitoring of the coagulation function has applications in many clinical settings. Routine coagulation assays in the clinic are sample-consuming and slow in turnaround. Microfluidics provides the opportunity to develop coagulation assays that are applicable in point-of-care settings, but reported works required bulky sample pumping units or costly data acquisition instruments. In this work, we developed a microfluidic coagulation assay with a simple setup and easy operation. The device continuously generated droplets of blood sample and buffer mixture and reported the temporal development of blood viscosity during coagulation based on the color appearance of the resultant droplets. We characterized the relationship between blood viscosity and color appearance of the droplets and performed experiments to validate the assay results. In addition, we developed a prototype analyzer equipped with simple fluid pumping and economical imaging module and obtained similar assay measurements. This assay showed great potential to be developed into a point-of-care coagulation test with practical impact.

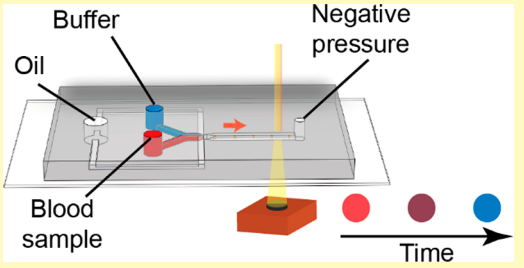

KEYWORDS: *blood coagulation, point-of-care testing, microfluidics, microfluidic viscometer, in vitro diagnostics*

Coagulation monitoring is an essential diagnostic need in many clinical settings. For example, before cardiovascular and other certain surgeries, coagulation testing may be required to stratify the bleeding or thrombosis risk and prescribe preventative measures accordingly.[1,2] After surgeries, coagulation function should be monitored given the high occurrence of postoperative acquired coagulopathy and its association with postoperative mortality.[3,4] In addition to perioperative care, clinical settings such as treatment of thrombosis or bleeding,[5] transfusion therapy,[6] and traumatic brain injury[7] also require coagulation monitoring. The means that gauging coagulation status rapidly and cost-effectively is of great significance in the management of these diseases and therapies.

Commonly accepted coagulation tests in clinics include prothrombin time (PT), activated partial thromboplastin time (aPTT), and thrombin time (TT), among others.[5] Despite the established clinical protocols developed over time, there are a few limitations associated with these tests. These tests generally used blood plasma as the testing sample and thus failed to incorporate the contribution of cellular components to blood clotting. Isolation of plasma from whole blood also complicated the sample preparation process and inevitably introduced a delay to the tests. In addition, these tests have been mostly performed in a central laboratory with trained personnel, limiting their applicability in resource-limited settings such as community clinics and less developed areas.

Point-of-care devices assessing the viscoelastic properties of whole blood can potentially address these limitations. Indeed, commercially available devices, such as thromboelastography (TEG) and rotational thromboelastometry (ROTEM), have been gradually getting acceptance.[8] Both TEG and ROTEM adopted a similar principle: the space between a rotating part and a stationary transducer is filled with the blood sample, and when the blood sample is clotting and becomes more viscous, the transducer moves along with the rotating part. The temporal movement of the transducer is reported to reflect the kinetics of the clotting process. Given their merits of monitoring the whole blood clotting as well as moderate portability, TEG and ROTEM have been tentatively used in perioperative care to guide coagulation therapies.[8] Despite that, these devices hold the limitations of high cost, large footprint, low throughput, and high sample consumption.

Device miniaturization leveraging the emerging microfabrication and microfluidic technology holds the potential to develop assays with small size, low sample consumption, and low cost.[9] To this end, several works have reported the development of point-of-care coagulation monitoring devices.

Received: November 8, 2021
Accepted: April 28, 2022

For example, a few works reported the designs of microfluidic devices with embedded electrodes to measure the electrical impedance of blood during clotting and report coagulation function.[10−12] In addition to electrical properties, mechanical properties of the blood sample, particularly viscosity, have also been used as the measurement target to reflect coagulation status. Work has been reported to directly or indirectly measure blood viscosity using methods such as mechanical resonance,[13−16] acoustic scattering,[17−20] optical scattering,[21] and fluid mechanics.[22,23] These works demonstrated the possibility of developing miniaturized coagulation assays and their potential for point-of-care coagulation monitoring. Nevertheless, the reported methods either required bulky sample pumping units or complicated data acquisition instruments, making them suboptimal for clinical applications.

In this work, we developed a blood coagulation assay using microfluidics with a simple setup, easy operation, and good portability. The microfluidic device continuously generates droplets by negative pressure at the outlet, with the disperse phase being the mixture of blood sample and buffer. As the blood sample coagulates and becomes more viscous, the blood-to-buffer ratio in the resultant droplets changes accordingly. By continuously monitoring the color of the generated droplets using a camera, the flow rate ratio of the blood sample and buffer can be estimated, and the viscosity of the blood sample over time can be deduced. The viscosity tracing can then be used to interpret the functional status of the blood coagulation. We first performed calibration experiments to determine the relationship between imaged color and viscosity of blood droplets. To validate this coagulation assay, we compared our measurements with those from a commercial thromboelastography instrument, performed the assay on hyper- and hypocoagulating blood samples, and analyzed the correlation between our measurements and a standard coagulation assay. To explore the assay's translational applicability, we prototyped a portable analyzer featured vacutainer-based pumping and an economical imaging module, demonstrating its potential in clinical applications. Compared with other reported works, our method holds the merits of low sample consumption, low demand on instrumentation, and easy operation (Table S1). We envision this assay to potentially be deployed in clinical settings where point-of-care coagulation monitoring is needed.

METHODS

Device Design and Fabrication. The microfluidic device included two aqueous inlets and one oil inlet. The two aqueous phases mixed at the flow-focusing area and were pinched off into droplets, and the mixing ratio, and thus the sample viscosity, was decided by colorimetric analysis of the generated droplets. The widths of the buffer, sample, oil, and collecting channel were 37, 37, 27, and 159 μm, respectively, and the heights of the channels were 25 μm throughout. The microfluidic devices were fabricated by polydimethylsiloxane (PDMS) soft lithography using SU-8 photoresist on silicon wafers as molds. Fabrication of silicon molds was outsourced to a microfabrication company (Suzhou Research Materials Microtech Company, China). Upon arrival, SU-8 molds were treated with oxygen plasma (PDC-002, Harrick Plasma) for 1 min before being placed in a vacuum chamber with silane vapor for 5−6 h. PDMS prepolymer (Sylgard 184, Dow) with a 10:1 base-to-hardener ratio were mixed, degassed, and poured on SU-8 molds, before being degassed again and baked at 60 °C for 10 h. The cured PDMS was then peeled off from molds and cut into desired shapes. Holes with diameters of 3 mm were punched at inlets to serve as liquid reservoirs, and holes with a diameter of 0.8 mm were punched at the outlet to connect tubing. The PDMS slabs, as well as glass slides (10127101P-G, Citotest Labware), were then treated with oxygen plasma for 1 min, before being placed in contact and baked at 110 °C for 10 min to finish bonding. Rain repellent (Aquapel, Pittsburgh Glass Works) was then flushed into the channels briefly to turn the channel walls hydrophobic before being removed by flushing the channels with filtered fluorinated oil (NOVEC 7500, 3 M Company).

Specimen Handling. Blood specimens were collected at Shenzhen University General Hospital under a protocol approved by the Institutional Review Board of Health Science Center at Shenzhen University, with informed consents obtained from all volunteers. Blue-top vacutainer tubes (Improvacuter, Improve Medical) containing 3.8% sodium citrate were used for blood collection. Thrombin time was measured using a commercial coagulation instrument (CS-5100, Sysmex Corporation). Thromboelastography was performed using a commercial instrument (T5000, UD-Bio). Samples with hyper- or hypo-coagulation states were achieved by spiking baseline blood samples with anticoagulant heparin (H811552, Macklin Biochemical Co.; working concentration of 8 U/mL) and procoagulant aprotinin (R141091, Aladdin; working concentration of 80 μg/mL), respectively. Spiked samples were incubated at room temperature for 1 h before being recalcified and assayed.

Experiment Setup. In initial experiments, 40 μL droplet generation oil (1864006, Bio-Rad) and 30 μL buffer containing 42% glycerol with blue food dye were pipetted into the oil inlet and buffer inlet, respectively. Citrated blood samples were supplemented with 0.2 M $CaCl_2$ (C3306, Sigma-Aldrich) with a ratio of 17:1, and 34 μL recalcified blood sample was pipetted into the sample inlet. A lab-made syringe puller was used to supply negative pressure, as shown in Figure S1. By pulling a 30 mL syringe from 27 to 29 mL, a negative pressure of 6.99 kPa (relative to atmospheric pressure) was generated, as estimated by ideal gas law. Imaging was performed using an inverted microscope (ECLIPSE Ts2, Nikon) coupled with a camera (VEO-E 310L, Phantom). In calibration experiments, glycerol solution (G116205, Aladdin) of different viscosity was obtained by adjusting the concentration, and the viscosity values were obtained from tabulated experimental data.[24] Food dyes were supplemented for visualization. In the comparison experiments with thromboelastographpy, both assays were performed at 37 °C. A lab-made temperature control chamber using laser-cut acrylic, strip heater, and thermostat was used for temperature control. Other experiments were performed in an air-conditioned laboratory with temperate set at 25 °C.

Data Analysis. Images were analyzed using ImageJ (National Institute of Health, USA). Droplets were segmented in images, and the R, G, and B values of each pixel within the droplet region were used to calculate the color indices and the mean. The color index was calculated by applying principal component analysis on the pooled (R, G, B) vectors using MATLAB (MathWorks, Inc.).

Design of the Portable Analyzer. The portable analyzer consisted of a consumer-grade digital camera with 10,000× magnification (TipScope CAM, CVGC Tech Company) for image acquisition, a two-axis translation stage, a light source, and a tablet computer (H7, Cevana). Software with a graphic user interface was designed to communicate with the camera.

RESULTS

Design of the Coagulation Assay. The coagulation assay developed in this work monitors the viscosity of the blood sample during coagulation by continuously generating blood droplets using a specially designed microfluidic device. The device adopted a Y-shaped flow-focusing channel to generate droplets, with sample and buffer solution serving as the disperse phases, as shown in Figure 1a. The flow was driven by a nearly stable negative pressure (−7.0 kPa relative to 1 atm; Figure S1) at the outlet, with all inlets subject to atmospheric pressure. After droplet formation, the two solutions gradually mix due to the secondary flow within,[25] and the droplets

https://doi.org/10.1021/acssensors.1c02360
ACS Sens. XXXX, XXX, XXX−XXX

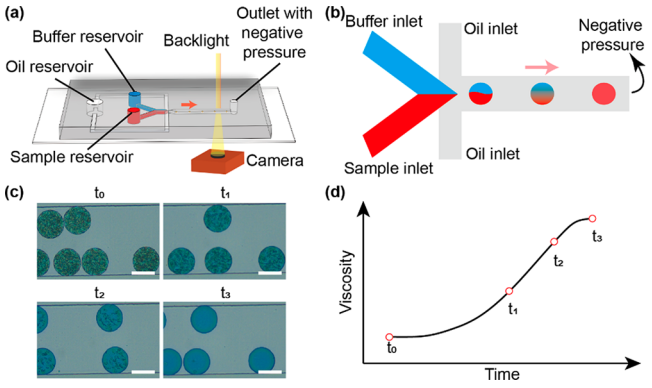

Figure 1. Overview of the coagulation device and working principle. (a and b) Schematic of the device and layout of the fluidic channels. Negative pressure is utilized to drive the flow, generating sample and buffer mixture-in-oil droplets. As the viscosity of the blood sample increases when coagulating, the sample-to-buffer volume ratio of the resultant droplets decreases accordingly, and the viscosity is calculated by colorimetric analysis. (c) Micrographs of the generated droplets at different time points into the assay. Scale bars, 50 μm. (d) Schematic of a typical viscosity tracing measurement of blood coagulation.

appeared homogeneous at roughly 7 mm downstream (Figure S2). In a typical assay, a citrated blood sample was recalcified, and 34 μL of the recalcified blood sample was immediately loaded into the device, before negative pressure was engaged to start generating droplets. As blood started coagulating and became more viscous, the flow rate of the blood sample decreased, while the flow rate of the buffer remained relatively constant, and the resultant droplets had relatively less blood sample within, exhibiting a less reddish and more bluish color (Figure 1b,c). By analyzing the color, the instantaneous viscosity of the blood during coagulation can be inferred.

Blood is normally regarded as a shear-thinning fluid. To examine whether we could neglect the non-Newtonian behavior and treat the blood sample as a Newtonian fluid, which would significantly simplify the calculation, we first sought to estimate the shear rate in our experiment setting. To achieve that, we first calculated the total flow rate of the buffer and sample phase by monitoring the droplet generation and the diameters of the resultant droplets. When the viscosity of the blood sample was at a baseline level (~4.0 cP), droplets with diameters of about 90 μm were generated at a frequency of 33 Hz (data not shown), resulting from a flow rate of about 5.2×10^6 $\mu m^3/s$ and an average velocity of about 2.8 mm/s for both phases. Therefore, the shear rate was approximately 100 s^{-1}. As the blood viscosity increased during coagulation, the shear rate that the blood sample experienced would be lower than 100 s^{-1}. In this shear rate regime, the viscosity would be relatively independent of the shear rate and the viscosity variation was lower than 10%.[26−28] Therefore, we neglected the non-Newtonian behavior of the blood in our assay and assumed that the flow rate of the blood phase was proportional to the inverse of the viscosity, following Hagen−Poiseuille equation.

The assumption that Hagen−Poiseuille equation applies in our experiment setting was further validated by experiments. We used a flow-focusing microfluidic device with single aqueous inlet to generate blood-in-oil droplets and simultaneously monitored the frequency and diameter of the formed droplets using a high-speed camera, aiming to calculate the flow rate of the blood sample in the channel of the blood phase (Figure S3a). As we adjusted the negative pressure at the outlet, the flow rate varied accordingly. As shown in Figure S3b, the results showed that the flow rate of the blood phase was proportional to the negative pressure applied at the outlet when the pressure was lower than 90 kPa, with $R^2 = 0.96$. Assuming a relatively consistent flow resistance distribution, the pressure drop from blood reservoir to the flow-focusing area should be proportional to the negative pressure applied at the outlet as well. Therefore, the results suggested that the flow rate of the blood phase was proportional to the pressure drop from the blood reservoir to the flow-focusing area and that the Hagen−Poiseuille equation indeed applied to our experiment settings.

Since both the sample reservoir and the buffer reservoir are subjected to atmospheric pressure, the pressure drop from the two reservoirs to the flow-focusing area are equal (Figure 1b). Therefore, the sample and buffer fluids in the two branch channels are driven by the same pressure drop, and the flow rate ratio of the two phases should be inversely proportional to the viscosity ratio, i.e., $Q_{blood}/Q_{buffer} \sim \mu_{buffer}/\mu_{blood}$. In addition, since the flow rate ratio of the two phases determines the composition of resultant droplets, by establishing the relationship between the color vector, flow rate ratio, and viscosity ratio, we could infer the instantaneous viscosity during blood coagulation, as shown in Figure 1d, through analyzing the color of the imaged droplets. The viscosity tracing could then be used to interpret the coagulation function using a similar principle as thromboelastography.

Calibration of the Measurements. We first aimed to investigate the relationship between the blood viscosity and the perceived color of the droplet images to obtain a calibration curve for future measurements. Ideally, the calibration experiments should be performed by adjusting the viscosity of the blood sample and analyzing the color of the resultant droplets accordingly. However, it was very challenging, if not impossible, to obtain blood samples of adjustable viscosities. Glycerol is colorless and water-soluble, and aqueous glycerol solutions of different concentrations provide clear solutions with varying viscosities. Therefore, we used aqueous glycerol solutions in calibration experiments where fluid viscosity needs to be adjusted.

The calibration was divided into two separate steps. First, we investigated the dependence of sample flow rate on sample viscosity ($Q-\mu$ relationship) using aqueous glycerol solutions. Since the $Q-\mu$ relationship is a fluid dynamics problem independent of the color appearance of the fluids, it should apply to blood samples as well. In the second step, we used a blood sample and studied the dependence of color appearance of droplets on the flow rate (color−Q relationship). Combining the $Q-\mu$ relationship and color−Q relationship, we could deduce the relationship between viscosity and color appearance (color−μ relationship), which would be used as the calibration curve for the calculation of blood viscosity in future measurements.

The experiments for the characterization of the $Q-\mu$ relationship were designed by applying Hagen−Poiseuille Law to the two branch channels of the glycerol solution and buffer solution. Since both reservoirs are exposed to the atmosphere, the pressure drop along these two branch channels are equal. Therefore, the flow rate ratio is supposed to be inversely proportional to the viscosity ratio, i.e., $Q_{glycerol}/Q_{buffer} \sim \mu_{buffer}/\mu_{glycerol}$. We prepared aqueous glycerol solutions with concentrations ranging from 39% to 71%, resulting in

https://doi.org/10.1021/acssensors.1c02360
ACS Sens. XXXX, XXX, XXX−XXX

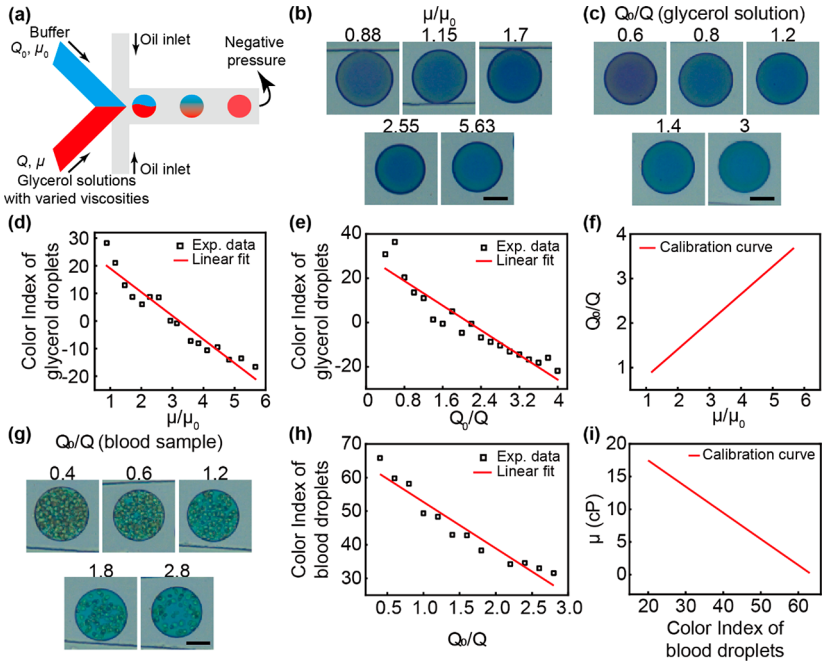

Figure 2. Calibration of the measurements. (a–f) Calibration of the relationship between viscosity and flow rate (Q–μ relationship). Glycerol with varied viscosities is used as the testing reagent (a), generating droplets with different color appearance (b). Droplets were also generated using different flow rates, showing different color appearances (c). The first principal component of the droplets' RGB value was adopted as the color index to fit the experiment results (d and e). Eliminating the color index gave the dependence of flow rate on viscosity (f). (g,h) Calibration of the relationship between flow rate and the color index of the generated blood droplets (color–Q relationship) using a similar method. (i) Resultant calibration curve of blood viscosity as a function of the color index of the generated blood droplets. Scale bars, 30 μm.

glycerol solutions with viscosities ranging from 3.05 to 19.53 cP at 25 °C. Nearly constant negative pressure was applied at the outlet to drive glycerol solution and buffer solution to generate droplets, as shown in Figure 2a. Directly measuring flow rates within the microfluidic channel was difficult. To address that, we added red dye to the glycerol solutions and blue dye to the buffer and used the color appearance to estimate the flow rate ratios. Glycerol solutions with different viscosity resulted in different mixing ratios with the buffer solution upon droplet generation, giving the resultant droplets different color appearances, as shown in Figure 2b. We then mixed glycerol solution and buffer solution with different volume ratios and generated droplets in a microfluidic channel for imaging, as shown in Figure 2c. The volume ratio for solution mixing was equivalent to flow rate ratios, $Q_{glycerol}/Q_{buffer}$, in terms of the preparation of droplets with different compositions.

We then sought to link the viscosity ratios to flow rate ratios through the color appearance of the two sets of droplets. Since RGB values are three-dimensional data, they require a strategy to reduce the RGB data to one dimension. A common practice is to convert the RGB value to grayscale following Grayscale = $0.299 \times R + 0.587 \times G + 0.114 \times B$. However, grayscale does not serve as a good metric to differentiate redness and blueness levels, since some reddish and bluish colors may end up with the same grayscale value. To define a metric to characterize the color appearance and separate imaged colors as far apart as possible, we pooled the three-dimensional RGB values of the two sets of droplets and performed principal component analysis. We defined the first principal component as the color index, which would be calculated as follows

$$\text{Color Index} = (0.87, -0.40, -0.30)\cdot(R, G, B) + 43.96 \quad (1)$$

where (R, G, B) represented the 8-bit color vector in RGB color space and the dot symbol represented the operation of the dot product. The first principal component explained 81.7% of the variances, suggesting that the color vectors from the two sets of experiments were in very similar color dimensions and that the color index calculated from eq 1 could adequately represent the colors. Compared to grayscale, the color index calculated from eq 1 provided a better one-to-one mapping from the blood–buffer ratio (Figure S4). We then performed linear regression using the least-squares method to find the viscosity ratio–color index relationship (Figure 2d) and the flow rate ratio–color index relationship (Figure 2e), respectively. The R^2 values of the linear fitting were 0.92 (n = 16) and 0.92 (n = 19), respectively, suggesting that relationships had good linearity. These two relationships were then used to deduce the Q–μ relationship, as shown in Figure 2f. The calculation showed that the Q–μ relationship followed

$$Q_0/Q = 0.62\cdot\mu/\mu_0 + 0.17 \quad (2)$$

where Q and μ were the flow rate and viscosity of the glycerol phase, respectively, and Q_0 and μ_0 were the flow rate and viscosity of the buffer phase, respectively. Equation 2 would apply to blood samples as well.

We then sought to characterize the color–Q relationship for the blood sample. We mixed blood sample and buffer solution with different volume ratios and generated droplets in microfluidic channels for imaging, as shown in Figure 2g. The volume ratio for solution mixing was equivalent to flow rate ratios, Q_{blood}/Q_{buffer}, in terms of the preparation of droplets with different compositions. We then performed multivariate linear regression to find the relationship between flow rates and the RGB values of the droplets, which gave

https://doi.org/10.1021/acssensors.1c02360
ACS Sens. XXXX, XXX, XXX–XXX

$$Q_0/Q = (-0.047, -0.030, 0.029)\cdot(R, G, B) + 4.33 \quad (3)$$

where Q is the flow rate of the blood phase. The R^2 of the fitting was 0.90 (n = 12), suggesting the linear fitting was valid. By normalizing the coefficient vector, we could define the color index for the droplets of the blood sample as

$$\text{Color Index} = (0.74, 0.47, -0.46)\cdot(R, G, B) \quad (4)$$

And the color-Q relationship for blood samples followed

$$\text{Color Index} = -13.8\cdot Q_0/Q + 66.5 \quad (5)$$

The experimental data and the fitted curve were plotted in Figure 2h. Substituting eq 2 into eq 5 and substituting μ_0 with the measured value of 3.44 cP gave the calibration equation for the color−μ relationship of

$$\mu = -0.40\cdot\text{Color Index} + 25.46 \quad (6)$$

as plotted in Figure 2i. μ is in the unit of cP, and Color Index is calculated from RGB values using eq 4.

Performance Validation of the Assay. Having calibrated the measurements, we performed experiments using blood samples to validate the assays. In the assay, citrated blood samples were recalcified by supplementing the blood sample with $CaCl_2$ solution to initiate coagulation. The recalcified blood sample was then loaded into the sample reservoir on the device immediately before the negative pressure was applied. Imaging was then started, typically at a rate of one frame every 10 s.

We first performed the assays on citrated blood samples that were recalcified and not recalcified, respectively. When the blood samples were recalcified, they gradually became more viscous, and the color appearance of the generated droplets transitioned from red to blue. By image analysis and calculation based on eqs 4 and 6), the viscosity over time during the coagulation process was obtained, as shown in Figure 3a. The

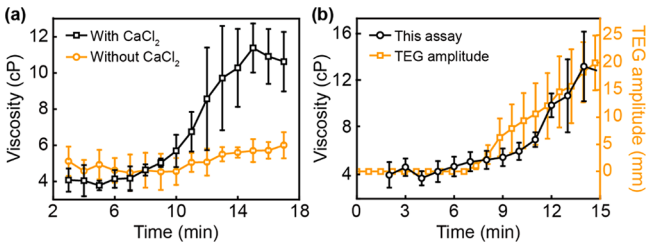

Figure 3. (a) Viscosity measurements of citrated blood samples supplemented with and without $CaCl_2$ using our device. (b) Comparison of measurements using this assay and a thromboelastography instrument. Data represent mean ± SD with n = 3.

measured viscosity in the initial stage was about 4 cP, which was within the normal range of 3.5−5.5 cP.[27] After about 7 min, the viscosity started to increase and reached 12 cP at roughly 15 min into the assay. In comparison, samples that were not recalcified showed a relatively constant viscosity. For example, the viscosity was measured as 5.1 ± 0.8 cP at the beginning of the assay and 6.0 ± 0.7 cP at the end of the assay, which were not significantly different (P > 0.05). We further compared our measurements with those from a commercial thromboelastography (TEG) instrument. As shown in Figure 3b, the viscosity tracing reported by our assay showed similar temporal dynamics as TEG tracing. These results showed that our assay was indeed capable of capturing the viscosity change during blood coagulation and offered comparable measurements with relatively more established instruments.

We then sought to examine whether our assay could differentiate hyper- and hypo-coagulable blood samples. We pretreated blood samples with baseline coagulation function using procoagulant, namely, aprotinin, and anticoagulant, namely, heparin, and performed the assays. As shown in Figure 4, Aprotinin-treated blood samples showed a faster

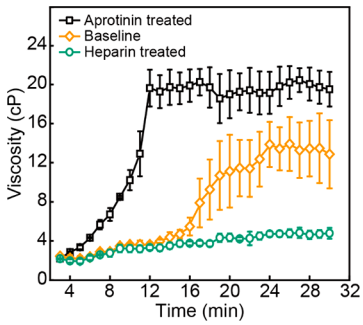

Figure 4. Viscosity measurements of blood samples treated with aprotinin (pro-coagulant) and heparin (anticoagulant). Data represent mean ± SD with n = 3.

coagulation progression, with the measured viscosity starting an upswing at roughly 4 min into the assay, which was much earlier than that of roughly 15 min from the baseline group. In addition, the viscosity quickly increased to 20 cP and plateaued. In contrast, blood samples treated with heparin showed a relatively constant viscosity, with a measurement around 4 cP throughout the assay, suggesting that the blood sample did not coagulate.

To explore the assay's potential in facilitating the gathering of clinical insights, we performed both our assay and standard coagulation tests on 11 patient samples (Figure 5a) and

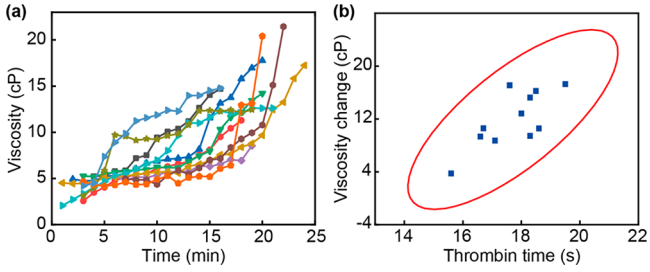

Figure 5. Viscosity measurements of 11 clinical samples. (a) Measured viscosity as a function of time. Data represent mean with n = 3. (b) Correlation between the viscosity change spanning the measurements and thrombin time measured from standard instruments. The red ellipse indicates 95% confidence. Pearson's correlation coefficient was 0.75 with P < 0.01.

performed correlation analysis. In particular, thrombin time represents the capability of the blood sample to convert fibrinogen into fibrin, which could be relevant to our measured viscosity. We defined viscosity change as the difference between the initial value and the peak value of the viscosity tracings and used this parameter as a metric for comparison. We then analyzed the correlation between viscosity changes derived from our measurements and thrombin times measured from the hospital laboratory. Results showed that samples with high thrombin time tended to have high viscosity change, with

https://doi.org/10.1021/acssensors.1c02360
ACS Sens. XXXX, XXX, XXX−XXX

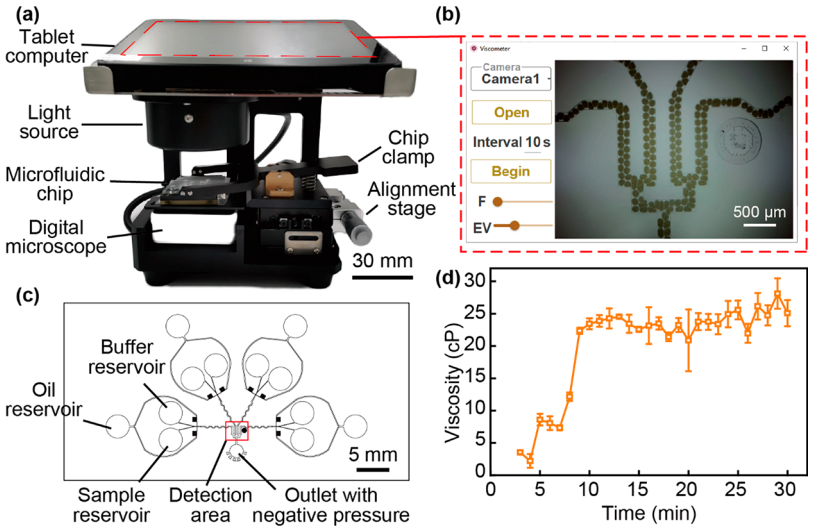

Figure 6. (a) Prototype analyzer developed for image acquisition and data analysis. (b) Graphic user interface designed for the analyzer with a representative micrograph acquired by the instrument during the measurement. (c) Design of the microfluidic device for multiple measurements. (d) Viscosity measurements of blood samples using the analyzer.

a Pearson's correlation coefficient of 0.75 ($P < 0.01$), indicating a strong correlation between these two measurements. These results suggested that there could be a link between the tendency of fibrin conversion and the viscosity of the resultant clot.

Development of a Portable Analyzer. To demonstrate our assay's potential of being translated into a point-of-care coagulation assay, we prototyped a portable analyzer to minimize human intervention in the assay, as shown in Figure 6a. The analyzer was mainly composed of a translational stage for chip immobilization, a zoom-in camera for image acquisition, and a tablet computer for user interfacing and data processing (Figure 6b). In addition, a vacutainer, which is an easily accessible consumable in hospitals, was used to provide negative pressure to drive the fluids, as shown in Figure S5. By prefilling a 3 mL vacutainer with 2.5 mL atmospheric air, the vacutainer provided a measured negative pressure of −15.6 kPa. We redesigned the microfluidic chip and incorporated multiple sample inlets, enabling simultaneous measurements of up to four samples (Figure 6c). The new channel design required the different negative pressure for fluid driving. The capability of scaling up is extremely useful when multiplex assays using different supplemental reagents are necessary. Since the new lighting condition and new camera resulted in different color appearances of the blood droplets, we additionally performed the measurement calibration using the same principle as mentioned above (data not shown). With the calibration curve, we performed the coagulation assay on blood samples using the prototyped analyzer, and the assay successfully reported the viscosity tracing (Figure 6d). The results demonstrated the potential of this assay as a point-of-care coagulation testing tool.

DISCUSSION AND CONCLUSIONS

In this work, we developed a microfluidic coagulation assay that continuously measured the viscosity of blood samples during clotting. The device generated droplets of blood and buffer mixture, and the composition of the resultant droplets changed as the blood became more viscous when coagulating, which could be inferred based on the color appearance. We characterized the color−viscosity relationship and performed the assay using blood samples to validate the assay efficacy. In addition, we developed a prototype of the portable analyzer which provided convenient fluid pumping, image acquisition, and data analysis. This coagulation assay could potentially be utilized as a point-of-care coagulation test with practical applications.

In the proposed method, we indirectly measured the blood viscosity based on the analysis of digital images. The random error in the measurements of the Color Index was roughly 8% in the experimental results. Based on eq 6, which suggests a linear dependence of the viscosity on the Color Index, the random error of the calculated viscosity should also be around 8%. In addition, we performed experiments to test whether the variation in the color of the original blood sample affects the results. A blood sample was used to generate droplets (without coagulation) at different time points, namely, 2, 3, 4, 6, and 13 h after blood draw, when the sample showed different color appearance due to the consumption of oxygen. The droplets showed a similar appearance in the captured images, and the calculated Color Indices were similar (Figure S6), suggesting that the color variation in the original blood sample had a negligible effect on the calculated Color Index and thus the viscosity.

Nevertheless, there are some limitations associated with the assay that shall be further addressed. First, the viscosity measurement showed a relatively small measurement range. Equation 2 indicates that the perceived viscosity change in response to flow rate change scales with $-1/Q^2$. When the viscosity is high, and the flow rate is low, random fluctuation in the flow rate could introduce high variance in the viscosity measurement. This limitation could potentially be alleviated by adjusting the viscosity of the buffer. Second, since the color appearance is highly dependent on the backlight as well as the ambient lighting, a more uniform backlight and a cover that blocks the ambient light shall be incorporated in the analyzer to provide consistent lighting. Lastly, the current form of the analysis neglected the non-Newtonian property of the blood samples. Though the results successfully captured the coagulation profile, a more rigorous analysis by factoring in

https://doi.org/10.1021/acssensors.1c02360
ACS Sens. XXXX, XXX, XXX−XXX

the shear-dependence of the blood viscosity shall be further developed in future work.

■ ASSOCIATED CONTENT

Supporting Information

The Supporting Information is available free of charge at https://pubs.acs.org/doi/10.1021/acssensors.1c02360.

Setup of the negative pressure generator, mixing process, setup of the prototype analyzer, and comparison with other methods (PDF)

Color change of the droplets during the experiment (MP4)

■ AUTHOR INFORMATION

Corresponding Author

Zida Li − *Department of Biomedical Engineering, School of Medicine and Guangdong Key Laboratory for Biomedical Measurements and Ultrasound Imaging, Department of Biomedical Engineering, School of Medicine, Shenzhen University, Shenzhen 518060, China;* orcid.org/0000-0002-1353-9414; Email: zidali@szu.edu.cn

Authors

Linzhe Chen − *Department of Biomedical Engineering, School of Medicine and Guangdong Key Laboratory for Biomedical Measurements and Ultrasound Imaging, Department of Biomedical Engineering, School of Medicine, Shenzhen University, Shenzhen 518060, China*

Donghao Li − *Department of Biomedical Engineering, School of Medicine and Guangdong Key Laboratory for Biomedical Measurements and Ultrasound Imaging, Department of Biomedical Engineering, School of Medicine, Shenzhen University, Shenzhen 518060, China*

Xinyu Liu − *Department of Biomedical Engineering, School of Medicine and Guangdong Key Laboratory for Biomedical Measurements and Ultrasound Imaging, Department of Biomedical Engineering, School of Medicine, Shenzhen University, Shenzhen 518060, China; Faculty of Information Technology, Collaborative Laboratory for Intelligent Science and Systems and State Key Laboratory of Quality Research in Chinese Medicines, Macau University of Science and Technology, Macao 999078, China*

Yihan Xie − *Department of Biomedical Engineering, School of Medicine and Guangdong Key Laboratory for Biomedical Measurements and Ultrasound Imaging, Department of Biomedical Engineering, School of Medicine, Shenzhen University, Shenzhen 518060, China*

Jieying Shan − *Department of Biomedical Engineering, School of Medicine and Guangdong Key Laboratory for Biomedical Measurements and Ultrasound Imaging, Department of Biomedical Engineering, School of Medicine, Shenzhen University, Shenzhen 518060, China*

Haofan Huang − *Department of Biomedical Engineering, School of Medicine and Guangdong Key Laboratory for Biomedical Measurements and Ultrasound Imaging, Department of Biomedical Engineering, School of Medicine, Shenzhen University, Shenzhen 518060, China*

Xiaxia Yu − *Department of Biomedical Engineering, School of Medicine and Guangdong Key Laboratory for Biomedical Measurements and Ultrasound Imaging, Department of Biomedical Engineering, School of Medicine, Shenzhen University, Shenzhen 518060, China*

Yudan Chen − *Department of Laboratory Medicine, Shenzhen University General Hospital, Shenzhen 518055, China*

Weidong Zheng − *Department of Laboratory Medicine, Shenzhen University General Hospital, Shenzhen 518055, China*

Complete contact information is available at: https://pubs.acs.org/10.1021/acssensors.1c02360

Author Contributions

Z.L. conceptualized and supervised the project. L.C. and D.L. fabricated the microfluidic devices and performed experiments. X.L., Y.X., J.S., H.H., and X.Y. designed and implemented the portable analyzer. Y.C. and W.Z. collected the blood samples and contributed to assay designs. L.C. and Z.L. analyzed the data. L.C. and Z.L. wrote the manuscript. All authors contributed to the manuscript.

Notes

The authors declare no competing financial interest.

■ ACKNOWLEDGMENTS

The authors thank Prof. Zhen Liang for insightful discussions on the data analysis. This work was supported by the Natural Science Foundation of Guangdong Province (Grant No. 2019A1515012010), Shenzhen Overseas Talent Program, and Shenzhen University Student Research Grants (Grant Nos. 470833 and 1021991).

■ REFERENCES

(1) Chee, Y. L.; Crawford, J. C.; Watson, H. G.; Greaves, M. Guidelines on the assessment of bleeding risk prior to surgery or invasive procedures. British Committee for Standards in Haematology. *British journal of haematology* **2008**, *140* (5), 496−504.

(2) Emani, S. M. Novel Coagulation Analyzers in Development: A Glimpse toward the Future of Microfluidics. *Semin Thromb Hemost* **2019**, *45* (3), 302−307.

(3) MacLeod, J. B.; Lynn, M.; McKenney, M. G.; Cohn, S. M.; Murtha, M. Early coagulopathy predicts mortality in trauma. *Journal of trauma* **2003**, *55* (1), 39−44.

(4) Devine, E. B.; Chan, L. N.; Babigumira, J.; Kao, H.; Drysdale, T.; Reilly, D.; Sullivan, S. Postoperative acquired coagulopathy: a pilot study to determine the impact on clinical and economic outcomes. *Pharmacotherapy* **2010**, *30* (10), 994−1003.

(5) Bates, S. M.; Weitz, J. I. Coagulation Assays. *Circulation* **2005**, *112* (4), e53−e60.

(6) Feltracco, P.; Serra, E.; Ori, C. Intra-operative transfusion management: the usefulness of point-of-care coagulation monitoring. *Blood Transfus* **2012**, *10* (3), 398−401.

(7) Genét, G. F.; Johansson, P. I.; Meyer, M. A.; Sølbeck, S.; Sørensen, A. M.; Larsen, C. F.; Welling, K. L.; Windeløv, N. A.; Rasmussen, L. S.; Ostrowski, S. R. Trauma-induced coagulopathy: standard coagulation tests, biomarkers of coagulopathy, and endothelial damage in patients with traumatic brain injury. *Journal of neurotrauma* **2013**, *30* (4), 301−6.

(8) Ganter, M. T.; Hofer, C. K. Coagulation Monitoring: Current Techniques and Clinical Use of Viscoelastic Point-of-Care Coagulation Devices. *Anesthesia & Analgesia* **2008**, *106* (5), 1366.

(9) Li, X.; Chen, W.; Li, Z.; Li, L.; Gu, H.; Fu, J. Emerging microengineered tools for functional analysis and phenotyping of blood cells. *Trends Biotechnol.* **2014**, *32* (11), 586−594.

(10) Ramaswamy, B.; Yeh, Y.-T. T.; Zheng, S.-Y. Microfluidic device and system for point-of-care blood coagulation measurement based on electrical impedance sensing. *Sens. Actuators, B* **2013**, *180*, 21−27.

(11) Maji, D.; Suster, M. A.; Kucukal, E.; Sekhon, U. D.; Gupta, A. S.; Gurkan, U. A.; Stavrou, E. X.; Mohseni, P. ClotChip: A Microfluidic Dielectric Sensor for Point-of-Care Assessment of

Hemostasis. *IEEE transactions on biomedical circuits and systems* **2017**, *11*, 1459.
(12) Duan, L.; Lv, X.; He, Q.; Ji, X.; Sun, M.; Yang, Y.; Ji, Z.; Xie, Y. Geometry-on-demand fabrication of conductive microstructures by photoetching and application in hemostasis assessment. *Biosens. Bioelectron.* **2020**, *150*, 111886.
(13) Xu, W.; Appel, J.; Chae, J. Real-time monitoring of whole blood coagulation using a microfabricated contour-mode film bulk acoustic resonator. *Journal of Microelectromechanical Systems* **2012**, *21* (2), 302−307.
(14) Cakmak, O.; Ermek, E.; Kilinc, N.; Bulut, S.; Baris, I.; Kavakli, I.; Yaralioglu, G.; Urey, H. A cartridge based sensor array platform for multiple coagulation measurements from plasma. *Lab Chip* **2015**, *15* (1), 113−120.
(15) Judith, R. M.; Fisher, J. K.; Spero, R. C.; Fiser, B. L.; Turner, A.; Oberhardt, B.; Taylor, R.; Falvo, M. R.; Superfine, R. Micro-elastometry on whole blood clots using actuated surface-attached posts (ASAPs). *Lab Chip* **2015**, *15* (5), 1385−1393.
(16) Erdoes, G.; Schloer, H.; Eberle, B.; Nagler, M. Next generation viscoelasticity assays in cardiothoracic surgery: Feasibility of the TEG6s system. *PLoS One* **2018**, *13* (12), e0209360.
(17) Viola, F.; Mauldin, F. W., Jr.; Lin-Schmidt, X.; Haverstick, D. M.; Lawrence, M. B.; Walker, W. F. A novel ultrasound-based method to evaluate hemostatic function of whole blood. *Clinica chimica acta; international journal of clinical chemistry* **2010**, *411* (1−2), 106−13.
(18) Nam, J.; Choi, H.; Kim, J. Y.; Jang, W.; Lim, C. S. Lamb wave-based blood coagulation test. *Sens. Actuators, B* **2018**, *263*, 190−195.
(19) Harder, S.; Santos, S. M. D.; Krozer, V.; Moll, J. Surface Acoustic Wave-Based Microfluidic Coagulation Device for Monitoring Anticoagulant Therapy. *Semin Thromb Hemost* **2019**, *45* (3), 253−258.
(20) Chen, X.; Wang, M.; Zhao, G. Point-of-Care Assessment of Hemostasis with a Love-Mode Surface Acoustic Wave Sensor. *ACS Sens.* **2020**, *5* (1), 282−291.
(21) Nadkarni, S. K. Comprehensive Coagulation Profiling at the Point-of-Care Using a Novel Laser-Based Approach. *Semin Thromb Hemost* **2019**, *45* (3), 264−274.
(22) Guler, M. T.; Isiksacan, Z.; Serhatlioglu, M.; Elbuken, C. Self-powered disposable prothrombin time measurement device with an integrated effervescent pump. *Sens. Actuators, B* **2018**, *273*, 350−357.
(23) Mena, S. E.; Li, Y.; McCormick, J.; McCracken, B.; Colmenero, C.; Ward, K.; Burns, M. A. A droplet-based microfluidic viscometer for the measurement of blood coagulation. *Biomicrofluidics* **2020**, *14* (1), 014109.
(24) sheely, M. L. Glycerol Viscosity Tables. *Industrial & Engineering Chemistry* **1932**, *24* (9), 1060−1064.
(25) Hudson, S. D. Poiseuille flow and drop circulation in microchannels. *Rheologica acta* **2010**, *49* (3), 237−243.
(26) Leo, J. A.; Simmonds, M. J.; Sabapathy, S. Shear-thinning behaviour of blood in response to active hyperaemia: Implications for the assessment of arterial shear stress-mediated dilatation. *Experimental Physiology* **2020**, *105* (2), 244−257.
(27) Nader, E.; Skinner, S.; Romana, M.; Fort, R.; Lemonne, N.; Guillot, N.; Gauthier, A.; Antoine-Jonville, S.; Renoux, C.; Hardy-Dessources, M.-D.; Stauffer, E.; Joly, P.; Bertrand, Y.; Connes, P. Blood Rheology: Key Parameters, Impact on Blood Flow, Role in Sickle Cell Disease and Effects of Exercise. *Frontiers in Physiology* **2019**, *10*, 1329.
(28) Reinke, W.; Johnson, P. C.; Gaehtgens, P. Effect of shear rate variation on apparent viscosity of human blood in tubes of 29 to 94 microns diameter. *Circulation research* **1986**, *59* (2), 124−32.

https://doi.org/10.1021/acssensors.1c02360
ACS Sens. XXXX, XXX, XXX−XXX